Peer-Reviewed Technical Communication

Very-High-Frequency Single-Input–Multiple-Output Acoustic Communication in Shallow Water

Jacob Rudander, Paul A. van Walree, *Member, IEEE*, Thor Husøy, and Pål Orten

***Abstract*—Very-high-frequency (VHF) underwater acoustic communication is a relatively unexplored terrain, but its importance is expected to increase with the growing demands for larger bandwidths and higher data rates. Knowledge of VHF propagation channels is a prerequisite to achieve high data throughput. In this paper, we present time-variant angle-resolved impulse responses for a set of 250-kHz shallow-water channels. The measurements were performed at high resolution using 64 hydrophones arranged in a line array. The measured channels are characterized by delay spreads of several milliseconds, Doppler spreads of tens of hertz, and angular spreads up to 30°. The angular spread is not separable from the delay-Doppler spread, and the impulse response depends heavily on the direction of arrival. Different beamforming and multichannel equalizer strategies are compared for a single-input–multiple-output configuration. A method combining subarray beamforming and multichannel equalization delivers in both noise- and interference-limited scenarios, transferring data at 78.125 kb/s over ranges up to 770 m.**

***Index Terms*—Acoustic communication, channel sounding, hydrophone arrays, SIMO, very high frequency, wideband systems.**

I. Introduction

HIGH-SPEED underwater acoustic communication is believed to play a central role in the rapidly emerging field of autonomous underwater vehicles and seabed sensor networks. Midrange (200–1000 m) solutions realizing data rates on the order of hundred kilobits per second (kb/s) could enable a new range of applications, such as real-time streaming of video, high-speed data harvesting, or serve as a cable replacement for, currently tethered, remotely operated vehicles. Nevertheless, such communication performance is so far unseen. Commercially available systems can deliver data rates on the order of a few tens of kilobits per second, whereas research systems have demonstrated rates of 500 kb/s [1] to 1 Mb/s [2], [3] in the megahertz band over short ranges and under controlled conditions.

A major problem for achieving high-speed communication at low frequency (LF) and midfrequency[1] (MF) is a small realizable bandwidth. Larger bandwidths can be realized in the very-high-frequency (VHF) band, but the migration is nontrivial. Absorption in seawater increases from a few decibels per kilometer to tens of decibels per kilometer [4], effectively reducing the maximum achievable range. Doppler shifts caused by platform motion and Doppler spread due to channel fluctuations are expected to increase in proportion to the carrier frequency. The scaling of the delay spread is less obvious. van Walree [5] shows an example of a markedly reduced delay spread when going from 4–5 to 7–8 kHz, whereas Rudander *et al.* [6] report 25 and 250 kHz delay profiles that are essentially the same. It is generally not possible to predict the VHF communication performance from measurements in lower bands.

Doppler compensation has proven valuable for low-rate coherent systems [7], and is also required for high-rate coherent systems in dynamic environments. A rule of thumb for successful adaptive channel tracking is $B_w T_b < 10^{-2}$ [8], where B_w is the Doppler spread and T_b is the symbol duration. The bandwidth of acoustic transducers typically scales with the resonance frequency so that larger bandwidths are available in higher transmission bands. The symbol rate $1/T_b$ thus increases with the carrier frequency of the signal, if indeed the full available bandwidth is used. High symbol rates allow faster channel tracking, thus mitigating the larger Doppler spread expected for VHF signaling. Therefore, Doppler tracking is not necessarily a bigger problem for VHF communications than it is for low-rate signaling. However, a different aspect of the increased symbol rate is that a given delay spread in milliseconds gets much longer when measured in filter taps. Large equalizers have slow convergence and may suffer from noise amplification. The VHF channel may put a high stress on the system to compensate for rapid fluctuations and the long effective channel. If the channel has sparse support, the effective length of the channel could be reduced using sparse channel estimation techniques [9]–[11].

A prominent equalizer design in the lower frequency range is the decision-feedback equalizer (DFE) with explicit phase tracking [12]. The DFE type has also been proven to work well in a VHF context [13], [14], demonstrating data rates of 87.769 kb/s using quadrature phase-shift keying (QPSK) over a 180-m shallow-water link. A single-channel equalizer is a powerful tool for mitigating channel distortions, but cannot exploit the spatial distribution of the signal.

Multipath propagation in a horizontal waveguide occurs over a range of vertical angles, denoted as the angular spread. Doppler spread and delay spread are two well-examined parameters (see, for example, [5], [6], and [15]–[17]), whereas angular spread is a less examined parameter. The reason is that the delay-Doppler spread is a sufficient description for a single hydrophone, whereas angular spread becomes a topic first with array receivers. Array processing techniques can alter the effective channel by modifying transmitter or receiver beam patterns, facilitating channel equalization by reducing the effective delay-Doppler spread. The angular spread is believed to become an increasingly important parameter in the VHF band, where additional

Manuscript received January 13, 2018; revised June 15, 2018; accepted July 5, 2018. This work was supported by Research Council of Norway. *(Corresponding author: Jacob Rudander.)*

Guest Editor: A. Sen Gupta.

J. Rudander is with Kongsberg Maritime, Horten 3183, Norway, and also with the University of Oslo, Oslo 0316, Norway (e-mail: jacob.hiden.rudander@kongsberg.com).

P. Orten is with Kongsberg Maritime, Kongsberg 3616, Norway, and also with the University of Oslo, Oslo 0316, Norway (e-mail: pal.orten@its.uio.no).

P. A. van Walree is with the Norwegian Defence Research Establishment, Horten 3183, Norway (e-mail: paul.vanwalree@ffi.no).

T. Husøy is with Kongsberg Maritime, Horten 3183, Norway (e-mail: thor.husoy@km.kongsberg.com).

Digital Object Identifier 10.1109/JOE.2018.2855298

[1]In this paper: LF < 1 kHz; MF 1–10 kHz, high frequency 10–100 kHz, and VHF > 100 kHz.

hydrophones can compensate for path loss without transceivers becoming impractically large.

For terrestrial communication, it was already suggested in [18] that narrow beams could reduce Doppler spread. This idea has recently got revitalized with the emergence of millimeter-wave communication [19], where it has been suggested to use directional antennas or beams. Va *et al.* [19]–[21] have shown that directional reception can increase the coherence time for narrowband signals in a channel described by the Clarke–Jakes model. Since each direction is mapped on a specific Doppler frequency shift, it is possible to reduce the spread of frequencies by filtering out signal components from undesired directions, effectively increasing the coherence time. Beamforming will also increase the signal-to-noise ratio (SNR) at the input of the receiver, and thereby compensate for path loss.

Underwater acoustic communication is (ultra)wideband as the bandwidth occupied by the signal is not small compared to the center frequency. Components arriving from different directions do not necessarily have independent fading. Scatterers are normally not uniformly distributed and scattering can be correlated [5]. Distinct paths with different vertical angles may have somewhat different Doppler shifts or different Doppler spreads. Therefore, the work described in [19]–[21] is not necessarily valid for the underwater acoustic channel.

Array processing has been used in different ways for underwater acoustic communication. In [22] and [23], a beamformer was used to separate different arrivals in an angularly sparse channel to achieve angular diversity, and thereby reduce complexity and enhance detection performance. Multichannel equalizers can also exploit angular diversity and have been used with good results in underwater acoustic communication, both for MF systems [24] as well as for systems partly within high frequency (HF) [25] and VHF [26], [27]. Choi *et al.* [26] achieved 83.2 kb/s (QPSK) over 530 m in a 14-m deep channel using a carrier of 100 kHz. Ochi *et al.*, using a carrier of 80 kHz, achieved 80 kb/s (QPSK) over 840 m and 120 kb/s (8-phase-shift keying) over 620 m in a slanted deep-water channel [27]. For LF, a combined beamformer multichannel equalizer structure was presented in [28]. The combined methods tend to have advantages over the pure multichannel equalization in terms of processing complexity.

The objectives of this paper are, first, to characterize signal dispersion in time, frequency, and angle for a wideband communication system with a center frequency of 250 kHz, and second, compare multichannel equalizers and combined beamforming/equalization strategies for a densely populated receive array. Angular dispersion is studied in particular to explain receiver performance. The data in this paper are from a specific type of VHF channel, namely the slanted midrange shallow-water channel, where a bottom-mounted transmitter is communicating to a moving antenna array receiver at the surface. The current focus is on high-speed communication in a single-input–multiple-output constellation, but the long-term goal of our study is to achieve full multiple-input–multiple-output (MIMO) communication in the VHF channel. The relevance of the measured channel characteristics is not limited to high-rate systems, but applies to a wide range of spectral efficiencies and SNRs.

The rest of this paper is organized as follows. Section II provides relevant background information and principles. Section III describes experiments conducted in August and November 2016. Section IV will discuss the angular distributions with focus on methods to use it. A description of the signal processing chain can be found in Section V. The results are presented in Section VI. Conclusions are finally drawn in Section VII.

II. Horizontal Underwater Acoustic Channels

The horizontal underwater acoustic channel is prone to multipath propagation, where signal copies are received via different paths. The signal at the receiver can be expressed as a sum of multipath components each arriving with a unique delay and channel interaction. For ultrawideband propagation, the channel interaction may be a frequency-dependent process, such as frequency-dependent absorption and surface loss. The impulse response for a frequency-dependent channel with N_{mpc} multipath components can be described by the ultrawideband channel model [29]

$$h(t,\tau)=\sum_{i=1}^{N_{\text{mpc}}} a_i(t)\chi_i(t,\tau)\circledast\delta(\tau-\tau_i) \tag{1}$$

where $\chi_i(t,\tau)$ is the time-varying path distortion, a_i is the gain, τ_i is the delay of the multipath components, and $\delta(t)$ is the Dirac delta function. The distortion $\chi_i(t,\tau)$ can represent effects such as frequency-dependent path loss and time-varying delays, which become important with wideband signaling.

Time variability causes Doppler spread, which can be described by the spreading function, also known as the deterministic scattering function [30]. It is defined as the Fourier transform of the impulse response

$$S(v,\tau)=\int_{-\infty}^{\infty} h(t,\tau)\exp(-2\pi \mathrm{i}vt)\mathrm{d}t. \tag{2}$$

The spreading function represents the distribution of received power as a function of the Doppler frequency shift and time delay. Integrating the spreading function with respect to frequency gives the power delay profile, or multipath intensity profile

$$P(\tau)=\int_{-\infty}^{\infty}|S(v,\tau)|^2\mathrm{d}v=\int_{-\infty}^{\infty}|h(t,\tau)|^2\,\mathrm{d}t \tag{3}$$

which represents the average power output as a function of time delay. If (2) instead is integrated over time delay, the Doppler power spectrum of the channel is given as follows:

$$P(v)=\int_{-\infty}^{\infty}|S(v,\tau)|^2\mathrm{d}\tau. \tag{4}$$

The above-mentioned equation represents the average power distribution over the Doppler frequency shift.

A. Angular Dispersion

While the channel impulse response (1) completely describes the time and frequency spread, it does not reveal the angular spread. Angular spread occurs in multipath channels, where signal copies arrive from different directions owing to refraction, reflection, and scattering. Equation (1) can be seen as the channel impulse response integrated over all angles. An angularly resolved model provides a more detailed description of the propagation

$$h(t,\tau,\theta,\varphi)=\sum_{i=1}^{N_{\text{mpc}}} a_i(t)\chi_i(t,\tau,\theta,\varphi)\circledast\delta(\tau-\tau_i) \tag{5}$$

where φ represents the azimuth angle and θ represents the polar angle. A one-dimensional array yields spatial resolution, which can be converted into an estimate of the impulse response resolved to a single angular dimension. For instance, for a vertical array

$$h(t,\tau,\theta)=\sum_{i=1}^{N_{\text{mpc}}} a_i(t)\chi_i(t,\tau,\theta)\circledast\delta(\tau-\tau_i). \tag{6}$$

Dette er en postprint-versjon / This is a postprint version.
DOI til publisert versjon / DOI to published version: 10.1109/JOE.2018.2855298

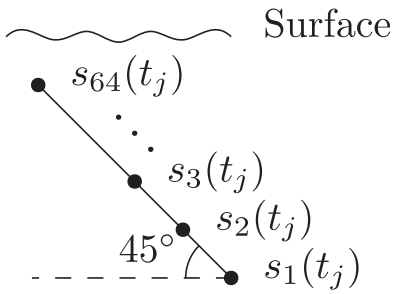

Fig. 1. Orientation of antenna array relative surface (upwards in figure).

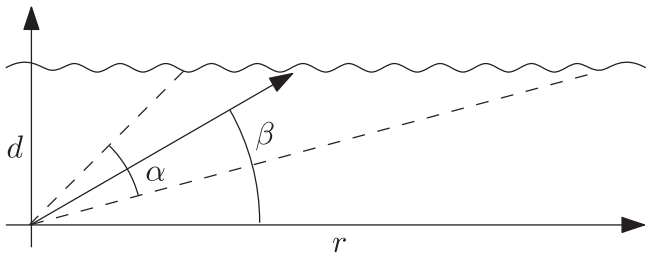

Fig. 2. Setup used for the measurements, where d is the water depth, r is the horizontal distance, α is the opening angle of the transmitter, and β is the orientation of the transmitter relative the seabed.

This is denoted as the time-variant angle-resolved impulse response in [31], but for simplicity it will here be referred to as the angular impulse response. Using (6), angularly resolved versions can be derived of the scattering function (2), the power delay profile (3), and the Doppler power spectrum (4). Directional transceivers result in different channels, depending on pointing direction and beamwidth. They may help to boost communication performance by listening in directions with reduced Doppler spread, to improve channel tracking, and/or in directions with a reduced delay spread to limit ISI and equalizer lengths. As the underwater acoustic communication is often time varying, flexible solutions require hydrophone arrays and explicit or implicit beamforming. An example of implicit beamforming is the multichannel equalizer, which can adaptively steer beams in directions of stable paths, and nulls in the direction of interference, in addition to equalizing the resulting channel.

III. Channel Measurements

Channel sounding experiments were conducted at two different occasions, in August and November 2016. The test locations were Horten inner harbor (experiment I and experiment II) and Breiangen (experiment III) both located in the Oslofjord in Norway. Horten inner harbor is a natural harbor surrounded by land and is at the widest point 2 km in diameter. The typical water depth in the central parts is 15 m with a soft seabed. Breiangen is an area in the middle of the Oslofjord outside Horten, with the typical depth of 200 m and 3.5 km away from the nearest land. Temperature and salinity were depth dependent, but a rough average over the water column yields about 60-dB/km absorption [4].

The setup consisted of a single transmitter with a 30° opening angle, attached to a rigid steel frame placed on the seabed. The receiver, 64 hydrophones arranged in a line array with a spacing ensuring no grating lobes (see Fig. 1), was mounted on a surface vessel. Fig. 2 depicts the slanted horizontal channel. The transmitter was oriented so that it was pointing in the same direction as the wind, this to allow the surface vessel to slowly drift off with the wind. The intention with the setup is to simulate a situation where a slowly moving surface vessel is communicating with a submerged platform or vehicle. The probing waveform was a binary phase-shift keying (BPSK) modulated periodic maximal-length (m-)sequence [32] transmitted head to tail, using a bit rate of 78.125 kb/s and a carrier frequency of 250 kHz. The source level was approximately 190 dB re 1 μ Pa^{2}m^2 for both experiments. A summary of the conditions for the various experiments can be seen in Table I.

TABLE I
Experimental Conditions and Parameters

Experiment	Month	Depth, d (m)	Probe (symbols)	Range, r (m)	Speed (m/s)	β (degrees)
I	Aug.	15	2047	200–600	0.3	30
II	Nov.	15	1023	200–800	0.16	0
III	Aug.	200	2047	200–1000	0.4	30

A. Computation

Channel sounding is a technique for measuring the channel impulse response, $h(t, \tau)$, as a function of time t and time delay τ, by transmitting dedicated probe signals through a channel. If the channel is linear and slowly time variant with respect to the channel probe, the estimate of the channel impulse response $\hat{h}$ is the true channel, $h(t, \tau)$ convolved with the ambiguity function of the channel probe $x(\tau)$

$$\hat{h}(t, \tau) = [h(t, \tau) \circledast x(\tau)] \circledast x^*(-\tau). \tag{7}$$

The closer the autocorrelation $x(\tau) \circledast x^*(-\tau)$ of the transmitted signal is to a true impulse, the better the estimate of the channel will be. Using repetitive channel probes, an estimate of the channel impulse $\hat{h}(t, \tau)$ will be available for $t_n = nT$, where T is the probe repetition period and $n \in [0, 1, 2, \ldots, N-1]$. To accurately capture the true channel, the repetition rate T^{-1} has to be selected with care. Temporal aliasing occurs when T is shorter than the delay spread, and frequency aliasing occurs when T^{-1} is smaller than the Doppler spread. m-sequence lengths of 1023 and 2047 were used, allowing measurements of Doppler spread up to 38 Hz and 76 Hz, and delay spreads up to 26 ms and 13 ms, respectively.

The impulse response estimate (7) is computed for each hydrophone m, and the angular response (6) is calculated by beamforming the individual responses. For a line array, using a delay-and-sum [33] beamformer, using continuous-time notation for convenience, the angularly resolved impulse response estimate can be expressed as follows:

$$\hat{h}(t, \tau, \theta) = \sum_{m=1}^{M} \hat{h}_m(t, \tau - \Delta_m) \exp(\mathrm{i}2\pi \Delta_m f_c) \tag{8}$$

where M is the number of hydrophones in the array, and $\Delta_m = x_m \cdot \sin(\theta)/c$ with x_m denoting the hydrophone's position in the array and θ is the angle of arrival. From (8), an angular delay-power spectrum estimate can be expressed as follows:

$$\hat{P}(\tau, \theta) = \int_0^{(N-1)T} \left|\hat{h}(t, \tau, \theta)\right|^2 \mathrm{d}t. \tag{9}$$

Similarly, an estimate of the angularly resolved Doppler spectrum reads

$$\hat{P}(v, \theta) = \int_0^{T} \left| \int_0^{(N-1)T} \hat{h}(t, \tau, \theta) \exp(-2\pi \mathrm{i} v t) \mathrm{d}t \right|^2 \mathrm{d}\tau. \tag{10}$$

Dette er en postprint-versjon / This is a postprint version.
DOI til publisert versjon / DOI to published version: 10.1109/JOE.2018.2855298

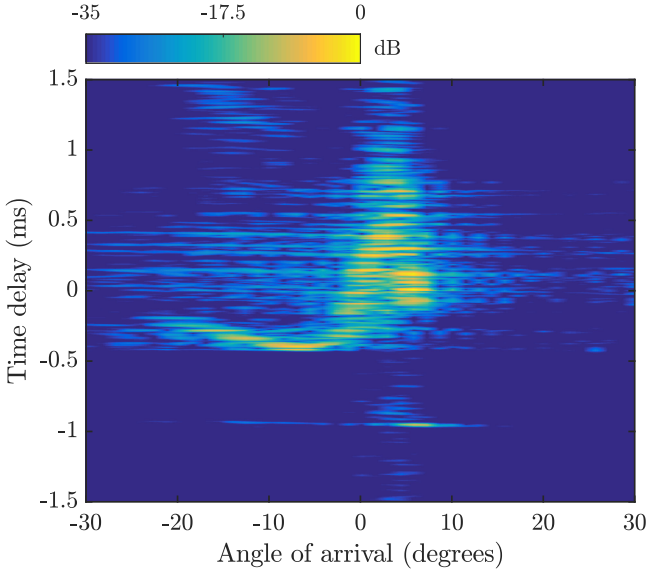

Fig. 3. Single m-sequence snapshot of the angular delay-power spectrum for experiment I at 200 m. The energy is normalized relative to the strongest arrival.

IV. Angular Distribution in an Underwater Acoustic Channel

In this section, we discuss the angular distribution for (ultra)wideband channels and methods to utilize it. We will be using examples from the shallow-water channel measured in experiment I (see Fig. 6).

In narrowband modeling of angular dispersion, it is common to assume that angle and delay are separable [29]. This assumption is not necessarily valid in ultrawideband communication, as demonstrated for a terrestrial channel in [34]. The same applies to our channel as illustrated by the VHF snapshot in Fig. 3 [(9) evaluated over one m-sequence]. The delay profile is different for different angles.

Another common assumption in narrowband modeling is that different directions are mapped onto discrete Doppler frequency shifts. It is, therefore, possible to reduce the Doppler spread of a signal by angular partitioning using narrow beams. This can be done to reduce fluctuations as a method to simplify receiver design. This method has been suggested in several papers [18]–[21]. If the same holds true in an underwater acoustic communication channel, then multipath components, through $\chi_i(t, \tau, \theta)$ [see (6)], should have unique Doppler frequency shifts for different θ, or at least a smaller Doppler spread compared with the response integrated over θ. Equivalently, different multipath components should vary more slowly in time compared to the summed response over a larger angular range. Interestingly, this is not what happens in our channel. The reason for this is the extension of the channel in time delay, where the Doppler shift depends not only on angle, but also on time delay. This is illustrated in Fig. 6(b), which shows the Doppler angular spectrum (10) for the data of Fig. 6(a). (Note that the nominal Doppler shift has been removed in the processing. The true Doppler spectrum peaks at about -50 Hz, corresponding to the receiver drift velocity of 0.3 m/s.) The frequency spread has a weak dependence on angle for the arrival cluster between 0° and 10°. The cluster below 0° has noticeably less Doppler spread. However, whether the latter direction is preferred for communications remains to be seen, because the received power is much lower than the power received between 0° and 10°. Angular partitioning, with the intention to reduce channels fluctuations, was tested in [35], showing a reduction only in specific directions.

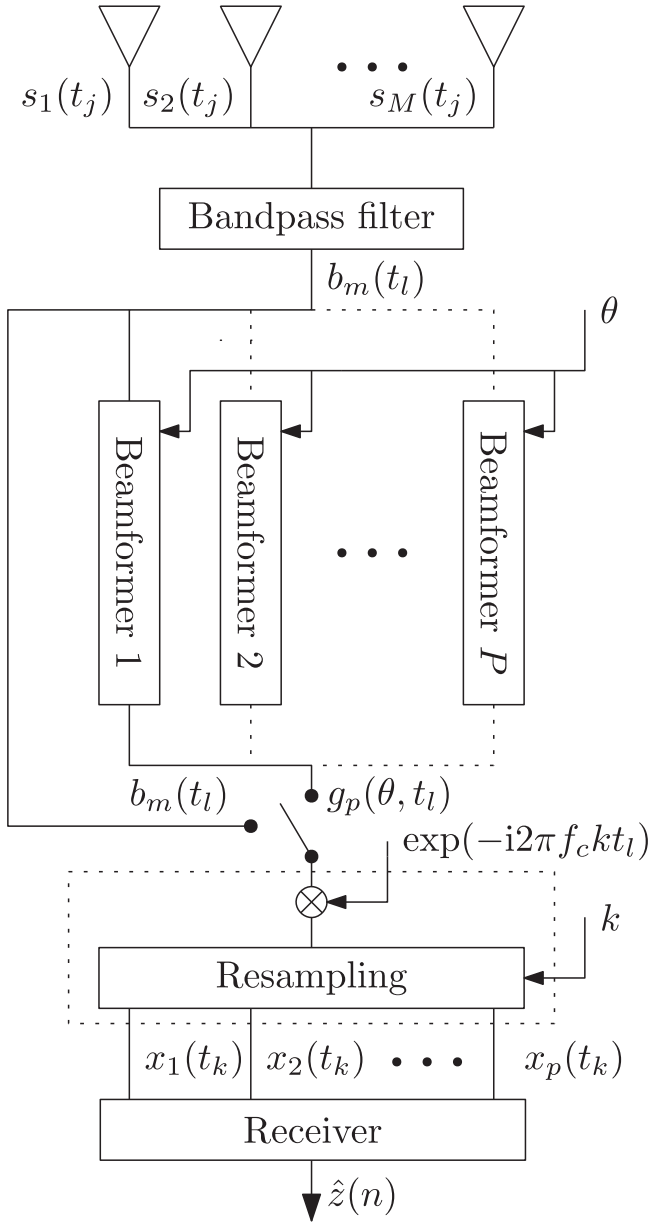

Fig. 4. Sketch of the signal processing chain.

A different possibility with narrow beams is to exploit the clustering of multipath components in time and angle appearing in many ultrawideband channels [29]. In [22], it was reported that the clusters were stable with a reduced Doppler distortion and the delay spread compared to the overall channel. Here, the authors steered beams toward different angular spread arrivals in an mid frequency (MF) deep-water channel, maintaining a low bit error ratio while reducing the overall receiver complexity. A similar method was used in [23] and [28], both cases with reported good performance in an MF channel.

Multichannel equalizers can adaptively steer beams in directions of stable paths and nulls in the direction of interference, in addition to equalizing the resulting channel. However, large arrays result in a high complexity, slow convergence, and noise amplification. A possible method to reduce the complexity is by sparse estimation methods [9]–[11], representing the channel response by only the most important taps. The clearly visible clustering in Fig. 3 indicates the opportunities for channel estimation methods exploiting sparsity in angle and/or delay.

Dette er en postprint-versjon / This is a postprint version.
DOI til publisert versjon / DOI to published version: 10.1109/JOE.2018.2855298

Sparsity is not examined further in this paper, whose scope is the impact of different hydrophone configurations.

A method addressing some of the problems related to large multichannel equalizers was presented in [36]. The hydrophone array was divided into subarrays, which were processed individually and whose soft output was combined coherently showing good results for an HF channel. This method results in set of smaller equalizers processing in parallel, which, depending on implementation, can reduce the overall complexity and improve convergence. A drawback of this method is that the subarray equalizers may fail to converge in scenarios with low input SNR. Beamforming the individual subarrays and feed the result to a common multichannel equalizer will increase the input SNR, but requires knowledge of the angular distribution. A combined subarray beamformer and multichannel equalizer was described in [37]. Here, the array was divided into several overlapping subarrays. Each subarray is beamformed, and the beams are fed to a multichannel equalizer. The documented performance is promising, especially at low SNR where it can take advantage of the beamforming gain that raises the equalizer input SNR. The size of the subarrays and the overlap is a tradeoff between the available computation power and the desired beamwidth. Large subarrays result in a reduced equalizer complexity, but also yield narrow beams that may require angular tracking.

We will in the remaining part of this paper compare different hydrophone configurations and beamformer–equalizer approaches.

V. Signal Processing

A schematic figure of the signal processing chain can be seen in Fig. 4. The acoustic waves are sensed by a hydrophone array. The analog signals are sampled and converted into the digital form, $s_m(t_j)$. The digital samples are first processed by a complex bandpass multirate filter converting the real passband signal into a decimated complex passband $b_m(t_l)$. Depending on the settings, the receiver can be operated in four different modes.

1) Single hydrophone: The beamformer is bypassed, and a hydrophone near the center of the array (#32) is processed with a single-channel equalizer.
2) Eight hydrophones: The beamformer is bypassed and eight hydrophones, evenly spread over the array [1:9:64], are processed with an eight-channel equalizer. Using the full-aperture maximizes the resolution, whereas our subarray spacing is small enough to keep grating lobes out of the angular interval where signal energy is present. A spacing of about three wavelengths was found to be optimal for the data analyzed in [24].
3) 64 hydrophones: The beamformer is bypassed and the full array is processed with a 64-channel equalizer. This receiver has many degrees of freedom, and given time to converge, it will be at least as good as any of the other methods. However, convergence may be poor, owing to the large number of taps. The use of a large least mean squares (LMS) step-size parameter, which speeds up convergence, results in noise amplification.
4) Eight subarrays: The beamformer is bypassed, and the array is split into eight interleaved subarrays ([1:8:57], [2:8:58], etc.) processed with eight parallel eight-channel equalizers, whose soft output is combined.
5) Single beam: Beamformer 0 steers a beam in the direction θ, using all hydrophones. The output is processed with a single-channel equalizer. Results are shown for a beam pointing to the direction of maximum signal power $\theta_{\max}$ and for the direction that maximizes the receiver output SNR θ_{opt}.

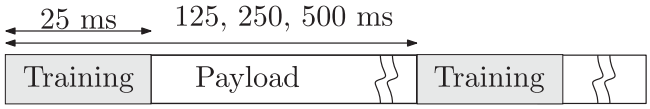

Fig. 5. Bit sequence.

6) Eight subarray beams: The array is divided into eight nonoverlapping eight-hydrophone subarrays, ([1:8], [9:16], etc.). Beamforming results in eight beams, which are processed by an eight-channel equalizer. Results are shown for beams pointing to the direction of maximum signal power $\theta_{\max}$ and for the direction θ_{opt} that maximizes the output SNR for the single-beam equalizer.

The dashed resampler block in Fig. 4 includes compensation for the nominal Doppler shift. This is done by resampling the signal with a constant factor k, and converting the complex passband signal into complex baseband using the Doppler compensated carrier frequency $k \cdot f_c$. The resulting data are fed to the receiver, a multichannel DFE with integrated phase-locked loop (PLL). The equalizer output is the symbol sequence $\hat{z}(n)$, which are estimates of the transmitted symbols $z(n)$. To compare different methods, we use the receiver output SNR [38]

$$\text{SNR}_{\text{out}} = \frac{\mathbb{E}(|z(n)|^2)}{\mathbb{E}(|\hat{z}(n)/\gamma - z(n)|^2)} \tag{11}$$

where $\gamma = \mathbb{E}(\hat{z}(n)/z(n))$ is equalizer bias.

A. Bit Sequence

Communication performance is evaluated by processing the channel probe signal, a cyclic m-sequence, as if it was a BPSK communication signal. The cyclic nature of the bit sequence limits the maximum effective delay spread to the m-sequence length. Longer delay spreads are aliased. Thus, communication performance measured on an m-sequence probe signal yields representative performance figures only if the channel delay spread is smaller than the m-sequence length. For the channels presented here, the delay spread is well within 13 ms, which is the duration of the shortest employed m-sequence (1023 symbols at 78.125 kb/s).

Signal portions with lengths of approximately 0.125, 0.25, and 0.5 s are considered, corresponding to data bursts of 10 000, 20 000, and 40 000 b. The first 2000 symbols are used for training, and the payload is equalized in the decision-directed mode (see Fig. 5). Longer bursts are generally more difficult to decode, as decision errors may cause a gradual deterioration of the equalizer state after initial training and convergence.

B. Beamformer

Direction of arrival estimation is performed by averaging the angular power distribution $P(\theta)$ over the training sequence, consisting of L samples

$$P(\theta) = \frac{1}{L}\sum_{l=1}^{L} g(\theta, t_l) g^*(\theta, t_l) \tag{12}$$

and the direction of arrival is defined as the angle of the peak power

$$\theta_{\max} = \arg\max_{\theta}(P(\theta)). \tag{13}$$

A simple wideband delay-and-sum beamformer [33] is used, steered toward $\theta_{\max}$. The beamformer uses uniform weighting and can handle 64 or 8 input signals. Because the data bursts are short, it is not necessary

to update the estimate of $\theta_{\max}$ within a burst. It suffices to perform the estimation at the start.

C. Conversion to Baseband and Resampling

A coarse estimate of the relative transmitter–receiver velocity is obtained by comparing the initial m-sequence with a bank of Doppler-shifted replicas. The estimated velocity V_0 gives a resampling factor

$$k = 1 - \frac{V_0}{c}. \tag{14}$$

This resampling factor is instrumental in the resampling in Fig. 4. Residual frequency offsets are handled by the PLL in the receiver, which is described in Section V-D.

D. Receiver

The input to the communication receiver in Fig. 4 is denoted by $\tilde{x}_p(t)$, where the index p denotes either a hydrophone channel or a beam. Acquisition is achieved with a filter matched to the m-sequence, where the signal start t_{det} is synchronized on the peak filter output. This synchronization is performed on one of the hydrophone channels (or beams), and on the first m-sequence of the received probe signal, resulting in a signal $x_p(t) = \tilde{x}_p(t - t_{\text{det}})$. Channel distortions are mitigated by a multichannel DFE, using P fractionally spaced ($T_{\text{b}}/2$, where T_{b} denotes the bit duration) feedforward filters with L_{ff} taps each, and a single feedback filter with L_{fb} taps. The available channels are stacked in a single column vector

$$\mathbf{y}_n = \left[\mathbf{b_n}^T, \mathbf{x}_{1,n}^T, \ldots, \mathbf{x}_{P,n}^T\right]^T \tag{15}$$

where

$$\mathbf{x}_{p,n} = \begin{bmatrix} x_p\left((n-1)T_{\text{b}} - \frac{(L_{\text{ff}}-1)T_{\text{b}}}{4}\right) \\ x_p\left((n-1)T_{\text{b}} - \frac{(L_{\text{ff}}-3)T_{\text{b}}}{4}\right) \\ \vdots \\ x_p\left((n-1)T_{\text{b}} + \frac{(L_{\text{ff}}-3)T_{\text{b}}}{4}\right) \\ x_p\left((n-1)T_{\text{b}} + \frac{(L_{\text{ff}}-1)T_{\text{b}}}{4}\right) \end{bmatrix} \exp\left[-\mathrm{i}\,\theta(n-1)\right] \tag{16}$$

and

$$\mathbf{b}_n = \begin{bmatrix} \tilde{z}(n-1) \\ \tilde{z}(n-2) \\ \vdots \\ \tilde{z}(n-L_{\text{fb}}+1) \\ \tilde{z}(n-L_{\text{fb}}) \end{bmatrix}. \tag{17}$$

Equalization yields symbol estimates

$$\hat{z}(n) = \mathbf{y}_n^T \mathbf{c}_{n-1} \tag{18}$$

using the LMS algorithm to update the equalizer coefficients

$$\mathbf{c}_n = \mathbf{c}_{n-1} + \delta\varepsilon(n)\mathbf{y}_n^* \tag{19}$$

where

$$\varepsilon(n) = \hat{z}(n) - \tilde{z}(n) \tag{20}$$

is the error signal, $\mathbf{c}_n$ is an equalizer with $PL_{\text{ff}} + L_{\text{fb}}$ taps, and δ is the LMS step-size parameter. The reference symbol $\tilde{z}(n)$ is given by

$$\tilde{z}(n) = \begin{cases} z(n), & \text{training} \\ \operatorname{sgn}\left\{\Re\left(\hat{z}(n)\right)\right\}, & \text{data.} \end{cases} \tag{21}$$

The filter is initialized with $\mathbf{c}_0 = \mathbf{0}_{PL_{\text{ff}}+L_{\text{fb}}}$.

Carrier recovery is performed with a PLL, comparing the phase angle of the equalized symbol $\hat{z}(n)$ with that of the reference symbol $\tilde{z}(n)$

$$\Phi(n) = \Im\left[\tilde{z}(n)^* \hat{z}(n)\right] \tag{22}$$

$$\theta(n) = \theta(n-1) + K_1\Phi(n) + K_2 \sum_{n'=1}^{n} \Phi(n') \tag{23}$$

where K_1 and K_2 denote the proportional and integral phase-tracking constants. The PLL is initialized with $\theta(0) = 0$.

A PLL is a low-complexity solution to combat time-varying Doppler shifts, which often yields adequate compensation for platform motion. It does not discriminate between paths in a multipath scenario, and a prerequisite for it to be effective is that the various paths dilate and contract in tandem. To a large extent, this condition is fulfilled in (slanted) horizontal waveguides with a limited angular spread. Travel time fluctuations due to platform motion can be strongly correlated between paths [5], resulting in correlated phases that can be effectively counterbalanced by a single PLL [39]. The PLL only corrects the phase offset due to the path dilation, not the dilation itself. Resampling with a time-varying resampling factor would be more proper wideband compensation method for path dilation [7], [39], but this is computationally less attractive than a PLL.

VI. Result and Discussion

The methods described in Section V are tested on data from the three experiments described in Section III. Since the impulse response differs between environments and between angular intervals within a given environment, there exists no single combination of filter lengths L_{ff} and L_{fb} that works well under all conditions. Instead, several combinations of L_{ff} and L_{fb} are tested, and the combination that yields the highest output SNR is reported. Low output SNRs often indicate that the equalizer fails to converge, or that it diverges in the decision-directed mode after initial convergence. Channels with a negative output SNR are marked with a dash (-).

The ranges described here are the horizontal range. For experiments I and II, the slant range is roughly similar to the horizontal range, whereas in experiment III it was 770 m.

A. Experiment I, 200 m

The angular delay power spectrum can be seen in Fig. 6(a). It consists of a weak direct arrival around 6° followed by a surface-reflected cluster between −20° and 0° and a highly energetic tail for positive angles. The signal power is smeared out over roughly 30° and represents the combined property of the acoustic channel and opening angle of the transmitter. The arrival is not consistent over angle with variations in time delay. Similarly, the Doppler spread in Fig. 6(b) also has an angular dependence. The surface reflection is difficult to discern in Fig. 6(b) because this power is smeared out in the Doppler domain.

Results from different equalizer and beamforming strategies are presented in Table II. The single hydrophone has the worst performance, receiving multipath components from the full angular range. The second worst method is a single beam in the $\theta_{\max}$ direction. A comparison of the angular delay power spectrum in Fig. 6 and beam pattern in Fig. 7 explains why; the strongest beam coincides with the largest delay-Doppler spread. The spatial filtering does not really reduce the delay-Doppler spread, compared to a single hydrophone. Fig. 7 also shows the output SNR for a single beam as a function of angle. Rather than coinciding with the highest energetic direction, the output SNR takes its highest values in the region with low delay-Doppler spread.

Dette er en postprint-versjon / This is a postprint version.
DOI til publisert versjon / DOI to published version: 10.1109/JOE.2018.2855298

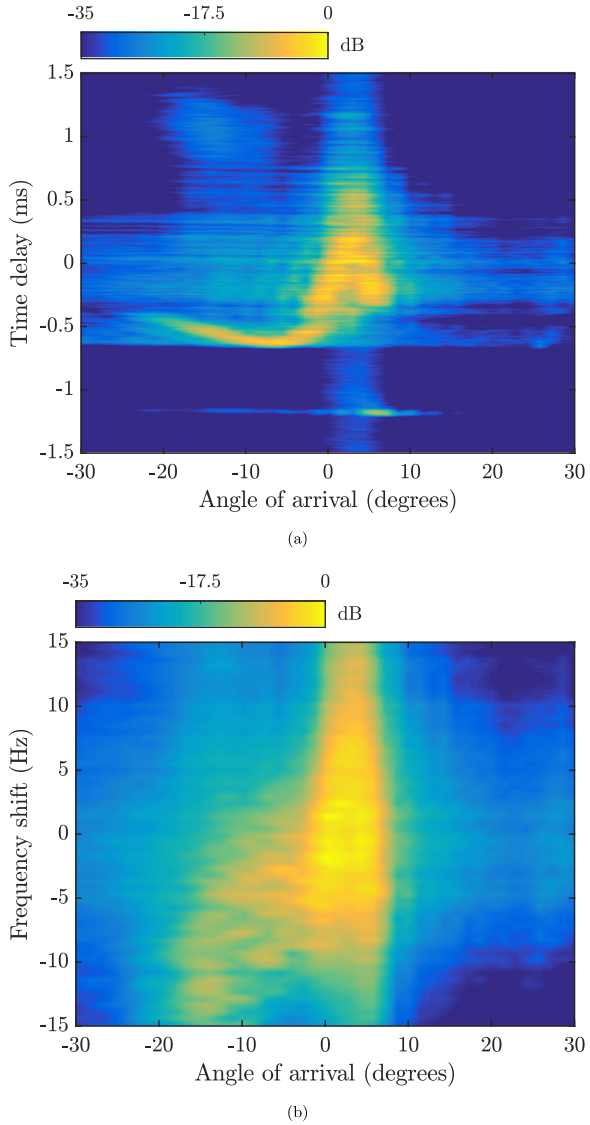

Fig. 6. Experiment I at 200 m. (a) Angular delay power spectrum. (b) Angular Doppler spectrum. Negative angles point toward the surface.

Although the optimal direction has a less energetic tail, it does not affect the length of the optimal equalizer much. The remaining methods work equally well, differing within ≈ 1 dB. The bit rate of the demodulated waveform is 78.125 kb/s, but the output SNRs indicate the feasibility of higher data rates through higher order constellations. Note that the number of filter taps can be large, even when the equalizer span in milliseconds appears short. For instance, the 64-channel equalizer has 64 feedforward sections of 1 ms, and 1 feedback section of 1 ms, corresponding to a whopping $64 \times 156 + 78 = 10\,062$ filter coefficients.

B. Experiment I, 300 m

The angular delay power spectrum and angular Doppler spectrum can be seen in Fig. 8. The angular spread is, similar to the shorter range, smeared over 30°, but the delay spread has increased for all directions. Both the Doppler angular spectrum and the angular delay power spectrum have a dip around 3°. This dip coincides with the highest output SNR direction in Fig. 9. In this example, the output

TABLE II
OVERVIEW OF OUTPUT SNR FOR DIFFERENT DATA BURST LENGTHS IN EXPERIMENT I AT 200 m

Comments	L_{ff} (ms)	L_{fb} (ms)	SNR_{out} (dB)		
			0.125 (s)	0.25 (s)	0.5 (s)
Single hydrophone	2	2	-	-	-
8 Hydrophones	2	2	14.8	13.6	12.3
64 Hydrophones	1	1	**15.4**	14.4	12.6
8 Subarrays	2	2	15.3	14.3	**13**
Single beam $\theta_{\max}$	2	2	-	-	-
Single beam θ_{opt}	2	2	12.0	8.6	-
8 Subarray beams $\theta_{\max}$	1	1	14.1	13.1	12.2
8 Subarrays beams θ_{opt}	1	1	**15.4**	**14.5**	12.6

L_{ff} is the equalizer feedforward filter length and L_{fb} is the feedback filter length. The bold values indicate the highest output SNR.

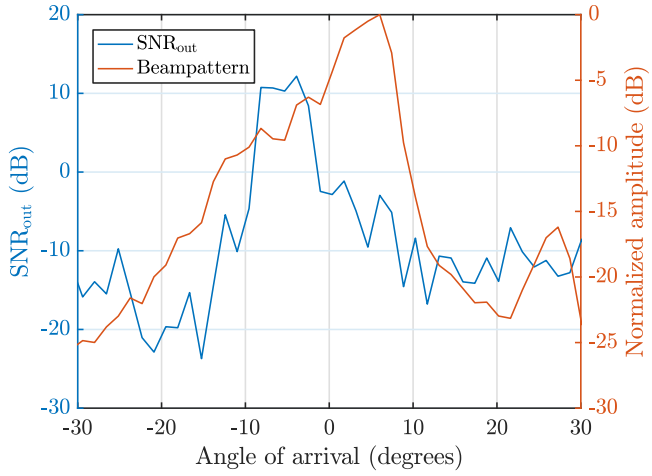

Fig. 7. Experiment I at 200 m, single-beam output SNR, left y-axis, and beam pattern, right y-axis, as a function of the angle of arrival. Negative angles point toward the surface.

SNR peaks within the main lobe of the beam pattern. The peak is narrow, rendering the performance of a single beam solution sensitive to pointing errors.

The result from different strategies can be seen in Table III. The multichannel equalizer and subarray solutions have within a few decibels range the same output SNR, whereas the single beam and single hydrophone perform much worse. The optimal single beam has almost 8 dB lower output SNR compared to the best solution for the shortest burst. In addition, it fails completely when the burst gets longer, indicating instability.

C. Experiment II, 190 m

Compared to the previous two examples, a quite different channel was experienced in experiment II. The test location was the same as in experiment I but at a different time of the year, and the transmitter had a more horizontal orientation. Fig. 10(a) shows that the received signal is spread over approximately 20° consisting of four diffuse bands in time delay, where all but the direct arrival at 10° are weak. The angular Doppler spectrum in Fig. 10(b) shows a small frequency spread for that arrival.

Dette er en postprint-versjon / This is a postprint version.
DOI til publisert versjon / DOI to published version: 10.1109/JOE.2018.2855298

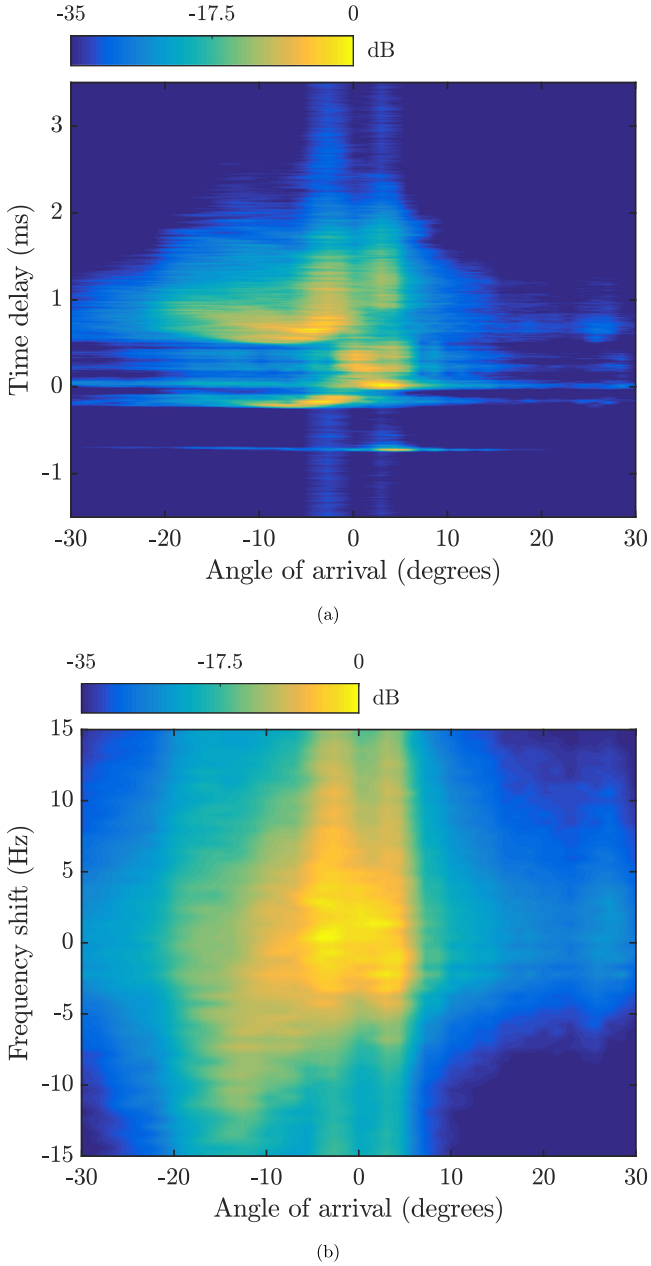

Fig. 8. Experiment I at 300 m. (a) Angular delay power spectrum. (b) Angular Doppler spectrum. Negative angles point toward the surface.

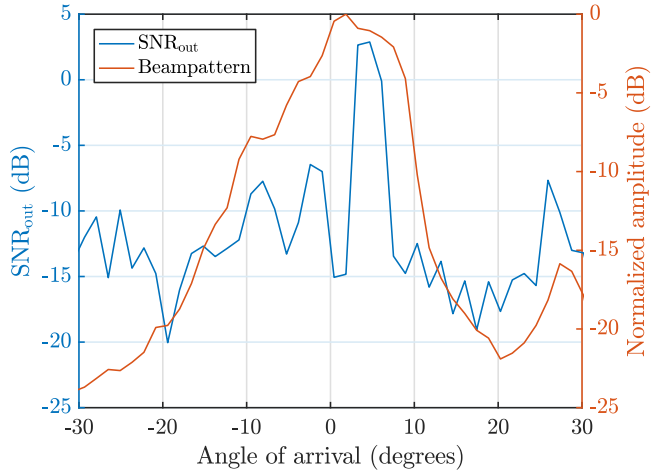

Fig. 9. Experiment I at 300 m, single-beam SNR, left y-axis, and beam pattern, right y-axis, as a function of the angle of arrival. Negative angles point toward the surface.

TABLE III
OVERVIEW OF OUTPUT SNR FOR DIFFERENT DATA BURST LENGTHS IN EXPERIMENT I AT 300 M

Comments	L_{ff} (ms)	L_{fb} (ms)	SNR$_{out}$		
			0.125 (s)	0.25 (s)	0.5 (s)
Single hydrophone	2	2	-	-	-
8 Hydrophones	2	2	14.3	12.6	11.2
64 Hydrophones	2	2	14.1	12.7	11.4
8 Subarrays	2	2	**14.6**	**13**	**11.8**
Single beam θ_{max}	2	2	-	-	-
Single beam θ_{opt}	2	2	6.7	0.4	-
8 Subarray beams θ_{max}	2	2	14.0	12.4	11.1
8 Subarrays beams θ_{opt}	2	2	13.8	12.2	11.0

L_{ff} is the equalizer feedforward filter length and L_{fb} is the feedback filter length. The bold values indicate the highest output SNR.

In this example, θ_{opt} coincided with θ_{max}, as seen in Fig. 11. Table IV provides the comparison for different methods. In contrast to the previous results, the multichannel equalizer with eight hydrophones is the second worst method. The reason for this is a particularly poor signal quality on hydrophone 1, which was most likely broken. The results in parenthesis in Table IV are the corresponding output SNR ignoring hydrophone 1. A significant increase in output SNR can be seen for the eight-channel equalizer. The other methods are fairly unaffected indicating more robustness to hydrophone failure.

The subarray equalizer performs comparably for θ_{max} and θ_{opt}, presumably because the two directions are close to each other, similarly to experiment I at 300 m. This channel is one of the few exceptions where the beam with the maximum power actually provides a channel stable enough to support communication.

It can also be noted that the SNR for several methods increases with increased frame length, indicating a stable channel that allows the equalizer to converge to the optimal solution.

D. Experiment II, 320 m

Here, the channel consists of four diffuse arrival clusters, spread over roughly 5 ms and 20° (see Fig. 12). A nonnegligible amount of energy is located in the tail, spread over a wide Doppler frequency range. Here, both the length and the Doppler spread of the channel would be fairly unaffected by arbitrarily steered narrow beams. The best direction is at the edge of the arrival (see Fig. 13). A comparison of different methods can be seen in Table V. This channel provides a considerable challenge for a communication system due to its fluctuating energetic tail that stretches over several hundreds of symbols. None of the methods handles these channel conditions particularly well, but there is a trend that multichannel adaptive methods utilizing all available hydrophones perform better. The 64-channel equalizer and the 8-beams equalizer yield a useful output SNR for the shortest burst.

Dette er en postprint-versjon / This is a postprint version.
DOI til publisert versjon / DOI to published version: 10.1109/JOE.2018.2855298

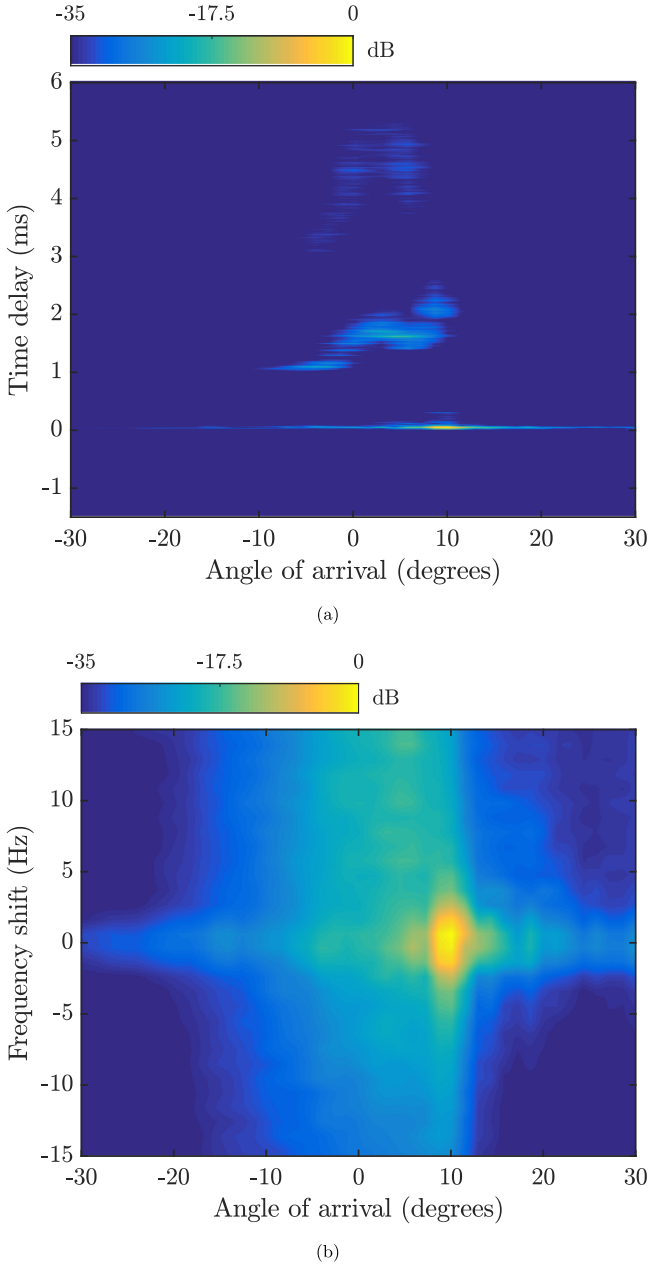

Fig. 10. Experiment II at 188 m. (a) Angular delay power spectrum. (b) Angular Doppler spectrum. Negative angles point toward the surface.

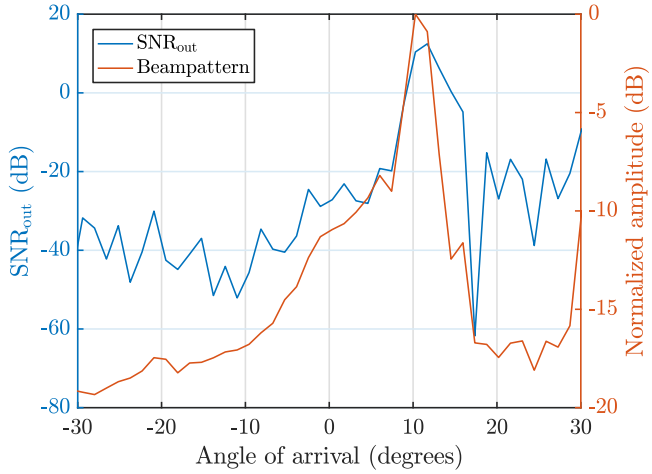

Fig. 11. Experiment II at 190 m, single-beam output SNR, left y-axis, and beam pattern, right y-axis, as a function of the angle of arrival. Negative angles point toward the surface.

TABLE IV
OVERVIEW OF OUTPUT SNR FOR DIFFERENT DATA BURST LENGTHS IN EXPERIMENT II AT 190 m

Comments	L_{ff} (ms)	L_{fb} (ms)	SNR$_{out}$ (dB)		
			0.125 (s)	0.25 (s)	0.5 (s)
Single hydrophone	8	1	-	-	-
8 Hydrophones	8	1	- (8.3)	- (9)	- (8.9)
64 Hydrophones	5	1	11.3 (11.5)	**11.8** (**12.4**)	**11.9** (**12**)
8 Subarrays	8	1	9.9 (10.2)	10.7 (11.2)	10.8 (11.4)
Single beam θ_{max}	0.5	1	8.1 (8.1)	7.8 (7.8)	7.2 (7.3)
Single beam θ_{opt}	0.5	1	10.3 (10.3)	10.0 (10.0)	9.6 (9.7)
8 Subarray beams θ_{max}	1	1	**11.7** (11.7)	**11.8** (11.8)	11.7 (11.7)
8 Subarrays beams θ_{opt}	1	1	**11.7** (**11.8**)	**11.8** (11.8)	11.7 (11.7)

L_{ff} is the equalizer feedforward filter length and L_{fb} is the feedback filter length. The results in parenthesis are after removing hydrophone 1.
The bold values indicate the highest output SNR.

E. Experiment III, 750 m

This experiment was conducted in a different area with a water depth of 200 m. This results in a channel quite different from the previous ones. Fig. 14 is characterized by a direct arrival, undisturbed by reflections from the seabed, and a weak surface reflection. The spread in time, frequency, and angle is small, indicating a stable channel. This channel is not limited by the intersymbol interference (ISI) as was the case with the other examples, but rather noise that puts a different constraint on the receiver.

The beam with the highest output SNR is also the strongest beam, i.e., $\theta_{\text{max}} = \theta_{\text{opt}}$ (see Fig. 15). Methods bypassing the beamformer perform poorly or converge slowly (64-hydrophone equalizer) (see Table VI). Methods involving the beamformer yield a useful output SNR for all frame lengths, presumably because they provide a sufficiently high input SNR to the equalizer, which converges more rapidly. The single-beam equalizer yields the highest output SNR. It is also noted that results slightly improve with increased frame lengths; this applies to all methods that do not yield a negative value. The stability of the channel allows the equalizer to converge further to the optimal solution. Fig. 16 illustrates this with the "instantaneous output SNR," computed by evaluating (11) over 0.1 s segments up to 4 s of data. The 64-channel equalizer achieves the highest SNR, given time to converge.

In this example, the single-beam method performs well for all three frame lengths. It may fail for very long frames, as the signal will eventually slip out of the main beam. Note that this is not the case for the rapid drop in the output SNR at 1.25 s in Fig. 16, which is caused by accumulated decision errors. The subarray methods have wider beams, and the 64-channel equalizer has the ability to steer beams and might be able to track arrivals in the angular domain by adaptive beamforming.

F. Discussion

Several methods with different performances and complexities have been evaluated in two shallow-water environments and one deep-water environment. The single-hydrophone method failed in all channels,

Dette er en postprint-versjon / This is a postprint version.
DOI til publisert versjon / DOI to published version: 10.1109/JOE.2018.2855298

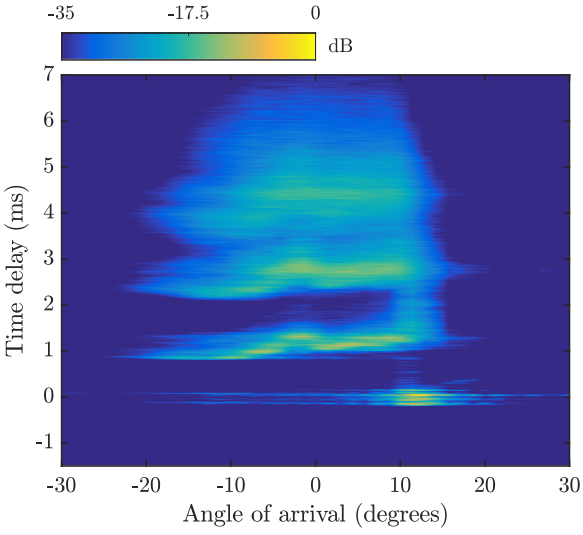

(a)

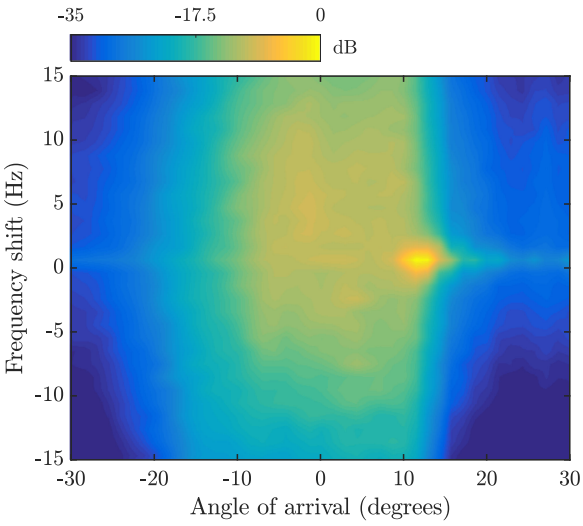

(b)

Fig. 12. Experiment II at 320 m, single-beam output SNR, left y-axis, and beam pattern, right y-axis, as a function of the angle of arrival. Negative angles point toward the surface.

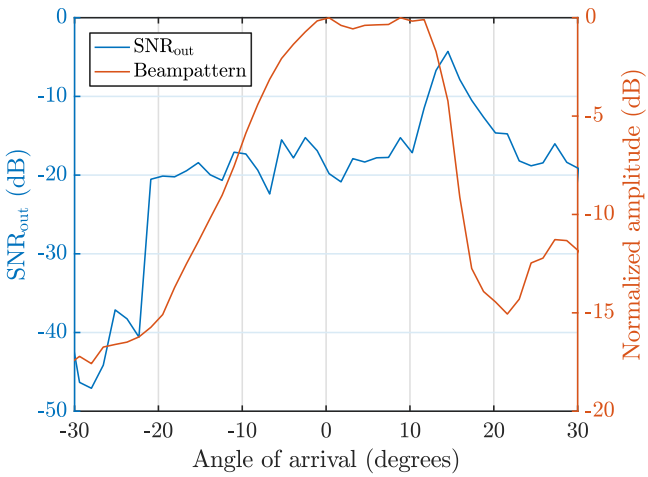

Fig. 13. Experiment II at 320 m, single-beam output SNR, left y-axis, and beam pattern, right y-axis, as a function of the angle of arrival. Negative angles point toward the surface.

TABLE V
OVERVIEW OF OUTPUT SNR FOR DIFFERENT DATA BURST LENGTHS IN EXPERIMENT II AT 320 m

Comments	L_{ff} (ms)	L_{fb} (ms)	SNR$_{out}$ (dB)		
			0.125 (s)	0.25 (s)	0.5 (s)
Single hydrophone	8	1	-	-	-
8 Hydrophones	8	1	2.5	-	-
64 Hydrophones	7	1	**4.8**	0.4	-
8 Subarrays	8	1	4.5	-	-
Single beam θ_{max}	8	1	-	-	-
Single beam θ_{opt}	8	1	-	-	-
8 Subarray beams θ_{max}	6	1	2.5	-	-
8 Subarrays beams θ_{opt}	6	1	4.4	**2.1**	-

L_{ff} is the equalizer feedforward filter length and L_{fb} is the feedback filter length. The bold values indicate the highest output SNR.

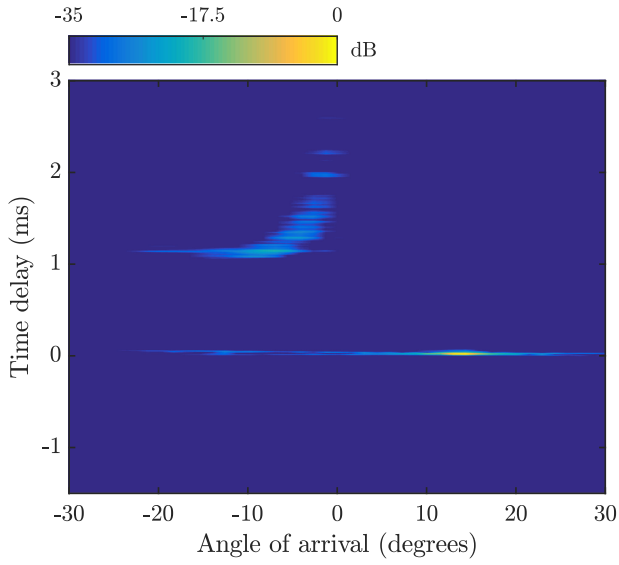

(a)

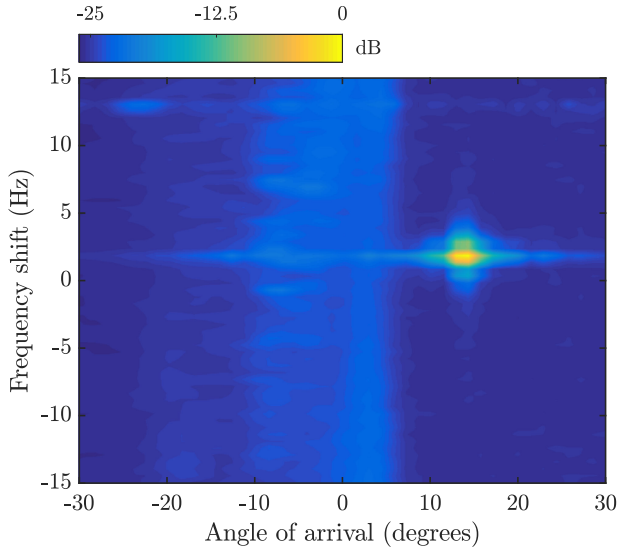

(b)

Fig. 14. Experiment III at 750 m, single-beam output SNR, left y-axis, and beam pattern, right y-axis, as a function of the angle of arrival. Negative angles point toward the surface.

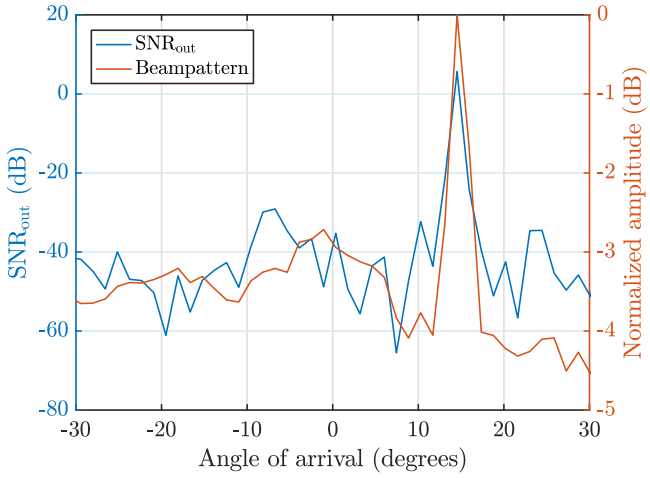

Fig. 15. Experiment III at 750 m, single-beam output SNR, left y-axis, and beam pattern, right y-axis, as a function of the angle of arrival. Negative angles point toward the surface.

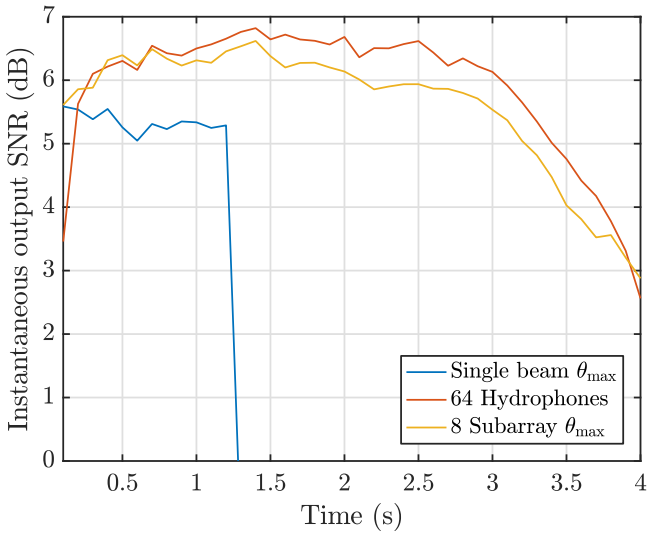

Fig. 16. Instantaneous output SNR as a function time.

TABLE VI
OVERVIEW OF OUTPUT SNR FOR DIFFERENT DATA BURST LENGTHS IN EXPERIMENT III AT 750 M

Comments	L_{ff} (ms)	L_{fb} (ms)	SNR$_{out}$ (dB)		
			0.125 (s)	0.25 (s)	0.5 (s)
Single hydrophone	2	1	-	-	-
8 Hydrophones	2	1	-	-	-
64 Hydrophones	2	1	3.4	4.5	5.3
8 Subarrays	2	1	-	-	-
Single beam θ_{max}	2	1	**6.1**	**6.1**	**6.1**
Single beam θ_{opt}	2	1	**6.1**	**6.1**	**6.1**
8 Subarray beams θ_{max}	2	1	5.7	5.8	**6.1**
8 Subarrays beams θ_{opt}	2	1	5.7	5.8	**6.1**

L_{ff} is the equalizer feedforward filter length and L_{fb} is the feedback filter length. The bold values indicate the highest output SNR.

whether limited by the ISI or by SNR. This indicates that a hydrophone array is necessary for reliable VHF communications.

Among the array solutions, the single beam steered toward the strongest arrival tends to fail in channels limited by ISI, but gives a decent result when a small delay-Doppler direction coincides with the strongest beam. A single beam steered in the optimal direction performs better by definition. However, the optimal direction was typically not stable over time. Furthermore, the optimal direction for the single beam tended to coincide with small delay-Doppler spread directions, which were not necessarily the directions yielding the highest input SNR. This is suboptimal in the sense that a significant fraction of the received energy is discarded.

Solutions where the beamformer was bypassed and channel data were sent directly to the equalizer(s) are adaptive. They do not require any information about the angular distribution of the channel. Although they can handle channels limited by ISI, they failed or performed worse in our low input SNR channel. Furthermore, they suffer from either high complexity, or they are less robust. The eight-channel equalizer failed completely when one of the channels was bad. The eight-channel equalizer (sparse array) can also suffer from grating lobes. In our measurements, the angular distribution did not coincide with more than one lobe, but for other channels signals can enter through grating lobes with reduced performance as a result.

The most stable method working under both ISI- and-SNR limited conditions was eight-beam subarray equalizer. This method is less sensitive to pointing errors, but requires *a priori* knowledge of the angular distribution to point the subarray beamformer in the correct direction. According to our results, the direction of maximum energy is a good starting point.

VII. CONCLUSION

The time-varying impulse response adequately describes the channel for single-element transceivers. Receiver arrays require an impulse response for each hydrophone, or alternatively a description in terms of the angle-resolved impulse response. The time-variant angle-resolved impulse response provides information about the spread in time, in frequency, and in angle. It is an important parameter for VHF channels, where array transceivers may be deployed to counterbalance the high propagation loss. Moreover, hydrophone arrays can effectively reduce the delay-Doppler spread experienced by receivers, for instance, by steering beams toward stable arrivals, and nulls toward fluctuating arrivals with a long delay.

In this paper, different methods have been evaluated to shape the apparent impulse response of the channel. A single beam followed by a single-channel equalizer is not necessarily a good choice, even when steered in the direction of maximum signal power. The reason is that the delay-Doppler spread can be large in this direction. A method that divides the receiving array into subarrays, feeding the subarray beams to a multichannel equalizer, is more robust and functions well in both SNR- and ISI-limited channels.

Subarray beamforming in combination with a multichannel equalizer enables shallow-water VHF signaling in the examined channels, yielding useful data rates and ranges. The required hardware would fit on sensor nodes and AUVs, and the low complexity of the LMS tracking algorithm may enable operation in real time. Further research is aimed at boosting the performance further through full MIMO.

ACKNOWLEDGMENT

The authors would like to thank K. Rimstad for assisting with channel measurements.

DOI til publisert versjon / DOI to published version: 10.1109/JOE.2018.2855298

REFERENCES

[1] A. Kaya and S. Yauchi, "An acoustic communication system for subsea Robot," in *Proc. OCEANS Conf.*, Sep. 1989, vol. 3, pp. 765–770.

[2] T. Riedl and A. Singer, "Towards a video-capable wireless underwater modem: Doppler tolerant broadband acoustic communication," in *Proc. Underwater Commun. Netw.*, Sep. 2014, pp. 1–5.

[3] J. Younce, A. Singer, T. Riedl, B. Landry, A. Bean, and T. Arikan, "Experimental results with HF underwater acoustic modem for high bandwidth applications," in *Proc. 49th Asilomar Conf. Signals, Syst. Comput.*, Nov. 2015, pp. 248–252.

[4] R. E. Francois and G. R. Garrison, "Sound absorption based on ocean measurements. Part II: Boric acid contribution and equation for total absorption," *J. Acoust. Soc. Amer.*, vol. 72, no. 6, pp. 1879–1890, Dec. 1982.

[5] P. A. van Walree, "Propagation and scattering effects in underwater acoustic communication channels," *IEEE J. Ocean. Eng.*, vol. 38, no. 4, pp. 614–631, Oct. 2013.

[6] J. Rudander, T. Husøy, P. Orten, and P. van Walree, "Shallow-water channel sounding for high speed acoustic communication," in *Proc. OCEANS Conf.*, Jun. 2017, pp. 1–8.

[7] P. J. Gendron, "Shallow water acoustic response and platform motion modeling via a hierarchical Gaussian mixture model," *J. Acoust. Soc. Amer.*, vol. 139, no. 4, pp. 1923–1937, 2016. [Online]. Available: https://doi.org/10.1121/1.4943552

[8] M. Stojanovic, "Recent advances in high-speed underwater acoustic communications," *IEEE J. Ocean. Eng.*, vol. 21, no. 2, pp. 125–136, Apr. 1996.

[9] N. Ansari, A. Gupta, and A. S. Gupta, "Shallow water acoustic channel estimation using two-dimensional frequency characterization," *J. Acoust. Soc. Amer.*, vol. 140, no. 5, pp. 3995–4009, 2016. [Online]. Available: https://doi.org/10.1121/1.4967448

[10] A. S. Gupta and J. Preisig, "A geometric mixed norm approach to shallow water acoustic channel estimation and tracking," *Physical Commun.*, vol. 5, no. 2, pp. 119–128, 2012. [Online]. Available: http://www.sciencedirect.com/science/article/pii/S1874490711000681

[11] W. Li and J. C. Preisig, "Estimation of rapidly time-varying sparse channels," *IEEE J. Ocean. Eng.*, vol. 32, no. 4, pp. 927–939, Oct. 2007.

[12] M. Stojanovic, J. A. Catipovic, and J. G. Proakis, "Phase-coherent digital communications for underwater acoustic channels," *IEEE J. Ocean. Eng.*, vol. 19, no. 1, pp. 100–111, Jan. 1994.

[13] P. P. J. Beaujean, "A performance study of the high-speed, high-frequency acoustic uplink of the HERMES underwater acoustic modem," in *Proc. OCEANS Conf.*, May 2009, pp. 1–6.

[14] P. P. J. Beaujean, E. A. Carlson, J. Spruance, and D. Kriel, "HERMES—A high-speed acoustic modem for real-time transmission of uncompressed image and status transmission in port environment and very shallow water," in *Proc. OCEANS Conf.*, Sep. 2008, pp. 1–9.

[15] M. Caley and A. Duncan, "Investigation of underwater acoustic multipath Doppler and delay spreading in shallow marine environment," *Acoust. Aust.*, vol. 41, no. 1, pp. 20–28, Apr. 2013.

[16] T. C. Yang, "Characteristics of underwater acoustic communication channels in shallow water," in *Proc. OCEANS Conf.*, Jun. 2011, pp. 1–8.

[17] S.-M. Kim, S.-H. Byun, S.-G. Kim, and Y.-K. Lim, "Characterization of high-frequency underwater acoustic channel around 100 kHz in a shallow water," in *Proc. OCEANS Conf.*, Sep. 2016, pp. 1–5.

[18] R. H. Clarke, "A statistical theory of mobile radio reception," *Bell Syst. Tech. J.*, vol. 47, pp. 957–1000, 1968.

[19] V. Va, J. Choi, and R. W. Heath, "The impact of beamwidth on temporal channel variation in vehicular channels and its implications," *IEEE Trans. Veh. Technol.*, vol. 66, no. 6, pp. 5014–5029, Jun. 2017.

[20] O. Norklit and R. G. Vaughan, "Angular partitioning to yield equal Doppler contributions," *IEEE Trans. Veh. Technol.*, vol. 48, no. 5, pp. 1437–1442, Sep. 1999.

[21] D. Chizhik, "Slowing the time-fluctuating MIMO channel by beam forming," *IEEE Trans. Wireless Commun.*, vol. 3, no. 5, pp. 1554–1565, Sep. 2004.

[22] J. Li and Y. V. Zakharov, "Efficient use of space-time clustering for underwater acoustic communications," *IEEE J. Ocean. Eng.*, vol. 43, no. 1, pp. 173–183, Jan. 2018.

[23] S. Ijaz, A. Silva, and S. M. Jesus, "Arrival-based detection for underwater communication systems," in *Proc. Conf. Workshop Underwater Commun.*, Sep. 2012, pp. 1–10.

[24] M. Pajovic and J. C. Preisig, "Performance analysis and optimal design of multichannel equalizer for underwater acoustic communications," *IEEE J. Ocean. Eng.*, vol. 40, no. 4, pp. 759–774, Oct. 2015.

[25] D. Rouseff, M. Badiey, and A. Song, "Effect of reflected and refracted signals on coherent underwater acoustic communication: Results from the Kauai experiment (KauaiEx 2003)," *J. Acoust. Soc. Amer.*, vol. 126, no. 5, pp. 2359–2366, 2009. [Online]. Available: https://doi.org/10.1121/1.3212925

[26] J. W. Choi, R. J. Drost, A. C. Singer, and J. Preisig, "Iterative multichannel equalization and decoding for high frequency underwater acoustic communications," in *Proc. 5th IEEE Sensor Array Multichannel Signal Process. Workshop*, Jul. 2008, pp. 127–130.

[27] H. Ochi, Y. Watanabe, T. Shimura, and T. Hattori, "The acoustic communication experiment at 1,600 m depth using QPSK and 8PSK," in *Proc. OCEANS Conf.*, Sep. 2010, pp. 1–5.

[28] M. Stojanovic, J. A. Catipovic, and J. G. Proakis, "Reduced complexity spatial and temporal processing of underwater acoustic communication signals," *J. Acoust. Soc. Amer.*, vol. 98, no. 2, pp. 961–972, 1995.

[29] A. F. Molisch, "Ultrawideband propagation channels-theory, measurement, and modeling," *IEEE Trans. Veh. Technol.*, vol. 54, no. 5, pp. 1528–1545, Sep. 2005.

[30] A. Goldsmith, *Wireless Communications*, 1st ed. New York, NY, USA: Cambridge Univ. Press, 2005, pp. 82–92.

[31] R. Kattenbach, "Statistical modeling of small-scale fading in directional radio channels," *IEEE J. Sel. Areas Commun.*, vol. 20, no. 3, pp. 584–592, Apr. 2002.

[32] S. Golomb and G. Gong, *Signal Design for Good Correlation: For Wireless Communication, Cryptography, and Radar*. New York, NY, USA: Cambridge Univ. Press, 2005, pp. 81–90.

[33] D. H. Johnson and D. E. Dudgeon, *Array Signal Processing: Concepts and Techniques*, 1st ed. Upper Saddle River, NJ, USA: Prentice-Hall, 1993, pp. 114–117.

[34] A. S. Y. Poon and M. Ho, "Indoor multiple-antenna channel characterization from 2 to 8 GHz," in *Proc. IEEE Int. Conf. Commun.*, May 2003, vol. 5, pp. 3519–3523.

[35] J. Rudander, T. Husøy, P. van Walree, and P. Orten, "Array processing to mitigate channel fluctuations in high-speed shallow water communication," in *Proc. 4th Underwater Acoust. Conf. Exhib.*, Aug. 2017, pp. 1–4.

[36] J. Preisig, "Challenges and analysis of adaptive multichannel equalization for large-N arrays," in *Proc. 49th Asilomar Conf. Signals, Syst. Comput.*, Nov. 2015, pp. 239–243.

[37] T. C. Yang, "A study of spatial processing gain in underwater acoustic communications," *IEEE J. Ocean. Eng.*, vol. 32, no. 3, pp. 689–709, Jul. 2007.

[38] P. A. van Walree, "On the definition of receiver output SNR and the probability of bit error," in *Proc. MTS/IEEE OCEANS Conf.*, Jun. 2013, pp. 1–9.

[39] P. A. van Walree, T. Jenserud, and M. Smedsrud, "A discrete-time channel simulator driven by measured scattering functions," *IEEE J. Sel. Areas Commun.*, vol. 26, no. 9, pp. 1628–1637, Dec. 2008.

Jacob Rudander received the M.Sc. degree in engineering physics from Chalmers University of Technology, Göteborg, Sweden, in 2011. Currently as a industry-employed doctoral student working toward the degree in underwater acoustic communication.

Since 2011, he has been with Kongsberg Maritime, Horten, Norway. His research interest includes underwater acoustic communication and signal processing.

Dette er en postprint-versjon / This is a postprint version.
DOI til publisert versjon / DOI to published version: 10.1109/JOE.2018.2855298

Paul A. van Walree (M'08) received the M.Sc. and Ph.D. degrees in solid-state physics from Utrecht University, Utrecht, The Netherlands, in 1992 and 1997, respectively.

From 1998 to 2009, he was an Underwater Acoustician with The Netherlands Organisation for Applied Scientific Research, Delft, The Netherlands. In 2009, he became a Scientist at the Maritime Systems Department, Norwegian Defence Research Establishment (FFI), Horten, Norway. His research interests include digital underwater communications, channel characterization and simulation, and acoustic signal processing.

Thor Husøy received the M.Sc. degree in telecommunication from the Norwegian University of Science and Technology, Trondheim, Norway, in 1996.

In 1997, he was a Research Assistant with the Norwegian Defence Research Establishment, Horten, Norway. From 1998 to 2000, he was an Acoustic Engineer with Statkraft Grøner, Oslo, Norway. Since 2001, he has been with Kongsberg Maritime, Horten, Norway, in various positions. His research interests include underwater acoustic communication, positioning, and signal processing.

Pål Orten received the M.Sc. degree in telecommunications from the Norwegian University of Technology and Science, Trondheim, Norway, in 1989 and the Ph.D. degree in wireless communications from Chalmers University of Technology, Göteborg, Sweden, in 1999.

He is the Vice President of the Technology-Realtime, Kongsberg Maritime, Kongsberg, Norway. He also holds a part-time position as a Professor of Wireless Communications at the University of Oslo, Oslo, Norway. His research interests include channel coding, multiple access, multiuser detection, multiple-input multiple-output, and channel adaptation systems with application to satellite systems, cellular systems, wireless access systems, industrial wireless sensor networks, and underwater communication systems.

Dette er en postprint-versjon / This is a postprint version.
DOI til publisert versjon / DOI to published version: 10.1109/JOE.2018.2855298